Published on 08 May 2015. Downloaded by Changchun Institute of Optics, Fine Mechanics and Physics, CAS on 29/05/2016 11:59:29.

Journal of Materials Chemistry C

PAPER

View Article Online
View Journal | View Issue

Cite this: J. Mater. Chem. C, 2015, 3, 5566

Enhancement of pump efficiency for an organic distributed feedback laser based on a holographic polymer dispersed liquid crystal as an external light feedback layer

Lijuan Liu,[ab] Li Xuan,*[a] Guiyang Zhang,[ab] Minghuan Liu,[ab] Lifa Hu,[a] Yonggang Liu[a] and Ji Ma*[ac]

Received 15th March 2015,
Accepted 24th April 2015

DOI: 10.1039/c5tc00731c

www.rsc.org/MaterialsC

We report a low threshold, high energy conversion organic distributed feedback (DFB) laser based on a holographic polymer dispersed liquid crystal (HPDLC) grating as an external light feedback layer, specifically, by adopting an acrylate-based monomer with low functionality and a rubbed polyimide (PI) alignment layer. In such configuration, the phase separated LCs were aligned along the preferred direction, which gave an increased refractive index difference between the LC and the polymer, so it can provide better light feedback in the HPDLC layer. The pump efficiency for the laser, such as lasing output threshold and conversion efficiency, can be enhanced. The light loss, diffraction efficiency and driving voltage were also investigated for the HPDLC structures to identify the effects of the rubbing layer and monomer functionality.

1. Introduction

Distributed feedback (DFB) organic semiconductor lasers (OSLs) have been developed extensively based on their materials and resonator structures. Organic semiconducting materials exhibit strong absorption, wide absorption bands, small concentration quenching and capability of easy processing.[1] Efficient energy conversion could allow optical pumping by light emitting diodes[2] or inorganic laser diodes,[3] which is promising for compact laser applications.[4] DFB structures have desired resonator geometries due to low thresholds and single longitudinal mode emission as a result of the long gain path and high wavelength selectivity.[5] So far, DFB OSLs have been demonstrated using several approaches, such as electron beam lithography,[6] electron beam lithography,[7] hot embossing,[8] reactive ion etching, liquid imprinting[9] and interference ablation.[10] There are two kinds of structures that are commonly used. One is the grating structure engraved on the active layer[11] and the other is the active medium deposited on the corrugated substrate.[12] In these cases, the active layer acts as both the gain layer and the index modulation layer, which makes the coupling mechanism complex and the design of the waveguide core layer, such as its material or thickness, difficult.

A DFB laser with a single active semiconducting layer as the core layer and a holographic polymer dispersed liquid crystal (HPDLC) grating layer as the external feedback layer has a different configuration.[13] We can control the parameters of the active layer (as the gain medium and the waveguide core layer) and the HPDLC grating layer (as the feedback layer) separately to adjust the properties of the lasing output for the device.[13a] HPDLC gratings are fabricated by exposing a mixture composed of a photosensitive monomer and a LC to an interference field created by two coherent laser beams by the photopolymerization induced phase separation (PIPS) method. The alternating layers of the polymer and the phase separated LC are formed corresponding to the interference patterns.[14,15]

In HPDLCs, the averaged orientation of liquid crystal molecules is aligned along the grating vector direction, *i.e.*, orthogonal to the holographic planes.[14] For feedback lights propagating along the grating vector, the refractive index difference comes from the polymer (index n_p) and the phase separated LC (ordinary index n_o). These two values of index are very close and the typical difference[16] can be as low as 10^{-5}. Thus the effective light feedback for lasing output is not high. In this work, we present a DFB OSL using a HPDLC as the external feedback layer. Specially, A rubbed polyimide (PI) layer was adopted on the substrate to control the orientation of the phase separated LCs to increase the refractive index difference in the grating vector direction for light feedback. We also found that the effect of the PI alignment layer was related

[a] State Key Laboratory of Applied Optics, Changchun Institute of Optics, Fine Mechanics and Physics, Chinese Academy of Sciences, Changchun, 130033, China. E-mail: xuanli@ciomp.ac.cn
[b] University of Chinese Academy of Sciences, Beijing, 100049, China
[c] Liquid Crystal Institute, Kent State University, Ohio, 44240, USA. E-mail: jma2@kent.edu

This journal is © The Royal Society of Chemistry 2015

Published on 08 May 2015. Downloaded by Changchun Institute of Optics, Fine Mechanics and Physics, CAS on 29/05/2016 11:59:29.

to different functionalities of acrylate monomer(s). Through adopting a low functional monomer and using a rubbed PI alignment layer, the orientation of phase separated LCs can be along the direction of the holographic planes. Therefore the refractive index difference in the HPDLC feedback layer can be increased and the lasing performance can be enhanced.

2. Experimental

2.1 Device structure and materials

The device structure is illustrated in Fig. 1. The core layer of the proposed laser device is made from poly(2-methoxy-5-(20-ethyl-hexyloxy) *p*-phenyl-enevinylene) (MEH-PPV), which serves as a laser gain layer. While the bottom glass substrate and the HPDLC grating layer are used as cladding layers to form HPDLC-grating/MEH-PPV/glass substrate configuration as an asymmetric slab waveguide.[13a] Different from previous reports, we applied polyimide (PI) as an alignment layer to control LC alignment on the other glass substrate in some samples, as illustrated in Fig. 1b. The PI was mechanically rubbed unidirectionally by a piece of velvet cloth along the direction of the holographic planes (*z* axis). The solution of MEH-PPV (Jilin OLED Material Tech) in xylene (6 mg ml^{-1}) was deposited onto the bottom glass substrate by spin-coating (2000 rpm). The MEH-PPV layer thickness was controlled at 80 ± 2 nm by the spin-coating rate and confirmed by the Dektak profilometer. The cell gap, *i.e.*, the thickness of the HPDLC, was controlled by a Mylar spacer at 6 μm.

To form the HPDLC by the photo-induced phase separation method,[15] nematic LC TEB30A (n_o = 1.522, n_e = 1.692, Δn = 0.170, Slichem, 28 wt%), *N*-vinylpyrrolidone (NVP, Sigma-Aldrich, 10 wt%) as a solvent and a chain extender, co-initiator *N*-phenylglycine (NPG, Sigma-Aldrich, 1.5 wt%), photo-initiator Rose Bengal (RB, Sigma-Aldrich, 0.5 wt%) and the monomer (60 wt%) were mixed. In order to study the effect of different monomer functionalities,[17] difunctional acrylate monomer phthalic diglycol diacrylate (PDDA, Sigma-Aldrich, 30 wt%) and penta-functional acrylate monomer dipentaerythritol hydroxyl pentaacrylate (DPHPA, Sigma-Aldrich, 30 wt%) were adopted in mixture A with a monomer functionality of 3.5 while PDDA only (60 wt%) were prepared in mixture B with a monomer functionality of 2. The chemical structures of DPHPA and PDDA are shown in Fig. 2a and b, respectively. Different samples were prepared, as shown in Table 1. Samples **a1** and **a2** were made from mixture A and samples **b1** and **b2** were made from mixture B. To compare the effect of the PI alignment layer, samples **a2** and **b2** had a PI layer on the top glass substrate in the device while samples **a1** and **b1** did not have a PI layer in the device.

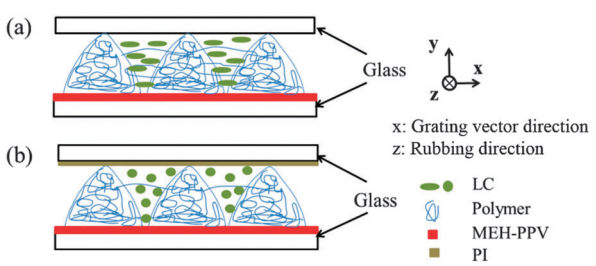

Fig. 1 Device structures of (a) without the PI alignment layer and (b) with the PI alignment layer.

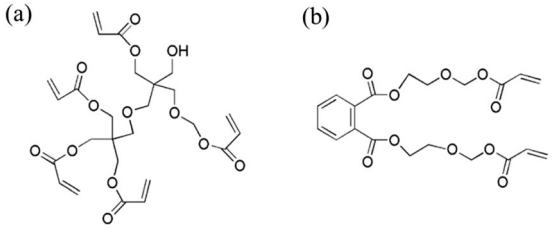

Fig. 2 Chemical structures of (a) DPHPA and (b) PDDA.

Table 1 Illustration and properties of samples

Sample #	Mixture	Top glass substrate	η_p (%)	η_s (%)	η_p/η_s
a1	A	Bare glass	56.5	1.3	43.5
a2	A	Coated with PI and rubbed	57.2	1.4	40.9
b1	B	Bare glass	55.5	2.9	19.1
b2	B	Coated with PI and rubbed	1.6	57.3	1/35.8

2.2 HPDLC fabrication and characterization

The mixture is injected into the empty cell by capillary action at room temperature (20–22 °C) after 12 h stirring at room temperature and put into the holographic optical field to form the HPDLC. The schematic optical setup is shown in Fig. 3. The cell was irradiated in the interference field created by two frequency-doubled, 532 nm continuous Nd-YAG laser beams. By changing the intersection angle (θ) of the two coherent beams,[14,15] the grating period (Λ) can be calculated and controlled according to $\Lambda = \frac{\lambda_{532}}{2\sin(\theta/2)}$. The period of the HPDLC grating was chosen at 590 nm for all the samples, which is used to achieve light feedback in the HPDLC *via* the third Bragg order for the gain MEH-PPV. The intensity of each recording beam was 4 mW cm^{-2}. The exposure time was 5 min and the cured grating area was 8 mm by 8 mm.

To characterize and compare the properties of HPDLCs with different structures, light loss and diffraction efficiency were analyzed. Decreased light loss can improve the energy conversion

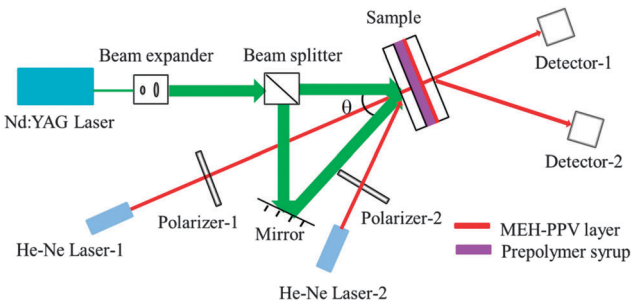

Fig. 3 Optical setup for fabrication and characterization of the HPDLC grating layer.

Published on 08 May 2015. Downloaded by Changchun Institute of Optics, Fine Mechanics and Physics, CAS on 29/05/2016 11:59:29.

efficiency of output laser. Light loss in different polarization states can also be used to indicate the orientation of the LC in the HPDLC. To calculate the light loss, during the fabrication process, a circularly polarized He–Ne laser (laser-1) was directed onto the sample in the normal direction using a polarizer (polarizer-1). Through rotating polarizer-1, the light loss (L') in the s or p polarization state is derived by $L' = (I_t - I_d)/I_t$. Here I_t is the intensity of He–Ne laser-1 passing through the sample before grating being fabricated and I_d is the intensity of He–Ne laser-1 detected using detector-1 in real time.

The diffraction efficiency of each sample was measured by another He–Ne laser. The laser beam from He–Ne laser-2 was incident onto the sample at the exact Bragg angle and the first order diffracted beam was measured by the detector-2. The Bragg diffraction angle was about 32° for our samples. The diffraction efficiency is defined as the diffracted light intensity in the first order divided by the incident light intensity. By rotating the polarizer-2, we can get diffraction efficiency in the s polarization state (η_s) or the p polarization state (η_p).

2.3 Lasing output performance

The holographically cured samples were then photo-pumped by a Q-switched frequency-doubled Nd:YAG laser (532 nm, 8 ns, 1 Hz). The pump beam was divided into two beams with equal intensity by a beam splitter. One beam was directed into a pulse energy meter and the other beam was shaped into a narrow strip (5 mm by 0.1 mm) by a cylindrical lens to the sample along the direction of the grating vector to pump the laser emission. The lasing output was detected and measured by a fiber pigtail detector coupled spectrometer (LabMax-TOP; Coherent Inc.). The lasing output, such as full width at half maximum (FWHM) and lasing threshold, can be obtained.

3. Results and discussion

3.1 Scattering loss in the HPDLC

The scattering loss can be used to determinate the goodness of the HPDLC grating as a feedback layer for lasing output. The lower the scattering loss, the more efficient the pump light, *i.e.*, the higher conversion efficiency of the pump input to the lasing output. The scattering loss in different polarization states can also give clues on LC orientation because scattering is mainly induced by the phase separated LC, which the refractive index of the phase separated LC mismatches with the refractive index of the environment of the polymer. Fig. 4 shows the scattering loss change with the HPDLC curing time for samples **a1–b2**. From Fig. 4a–c, we can see the scattering loss for p polarization light is greater than that for s polarization light for samples **a1**, **a2** and **b1** while from Fig. 4d, the scattering loss for s polarization light was larger than that for p polarization light. The scattering loss difference for different polarization states indicates that the LC orientation in the HPDLC is different. We will discuss this in Section 3.2.

3.2 Diffraction efficiency for the HPDLC

Fig. 5 shows the real-time diffraction efficiencies of each sample in different polarization states. In Fig. 5a–c a similar trend is shown, where the p light diffraction efficiency (η_p) is greater than the s light diffraction efficiency (η_s) for samples **a1**, **a2** and **b1**, whereas from Fig. 5d it is observed that the s light diffraction efficiency for sample **b2** is larger than p light diffraction efficiency during the HPDLC fabrication process. The diffraction efficiencies in different polarization states for each sample are listed in Table 1. For mixture A (DPHPA/PDDA based), the grating optical sensitivities (η_p/η_s) of **a1** and **a2** were 43.5 and 40.9, respectively. However, for mixture B (only PDDA based), the grating optical sensitivities η_p/η_s of **b1** and **b2** were

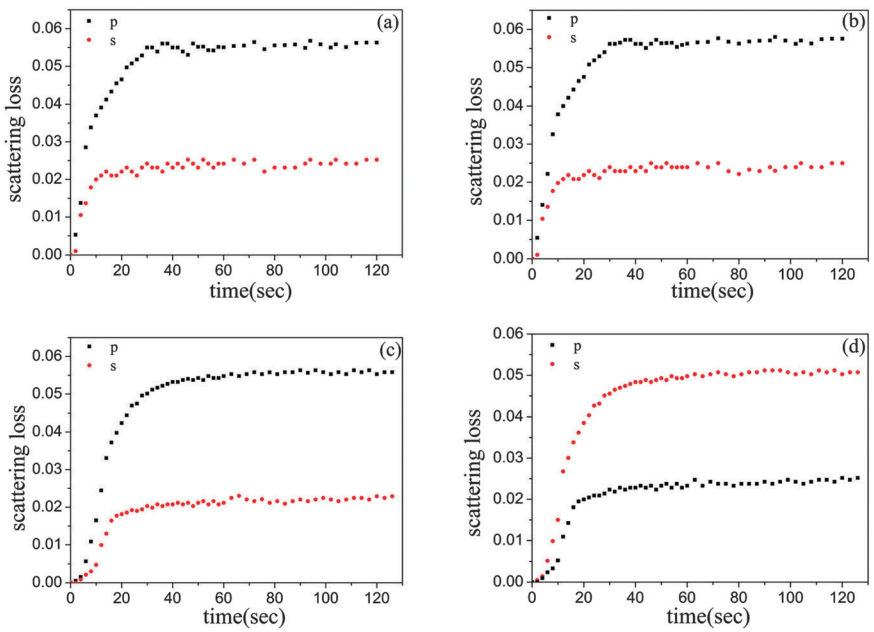

Fig. 4 Evolution of the light loss for p polarization (square) and s polarization (sphere) with curing time for (a) **a1**, (b) **a2**, (c) **b1** and (d) **b2**, respectively.

 This journal is © The Royal Society of Chemistry 2015

Published on 08 May 2015. Downloaded by Changchun Institute of Optics, Fine Mechanics and Physics, CAS on 29/05/2016 11:59:29.

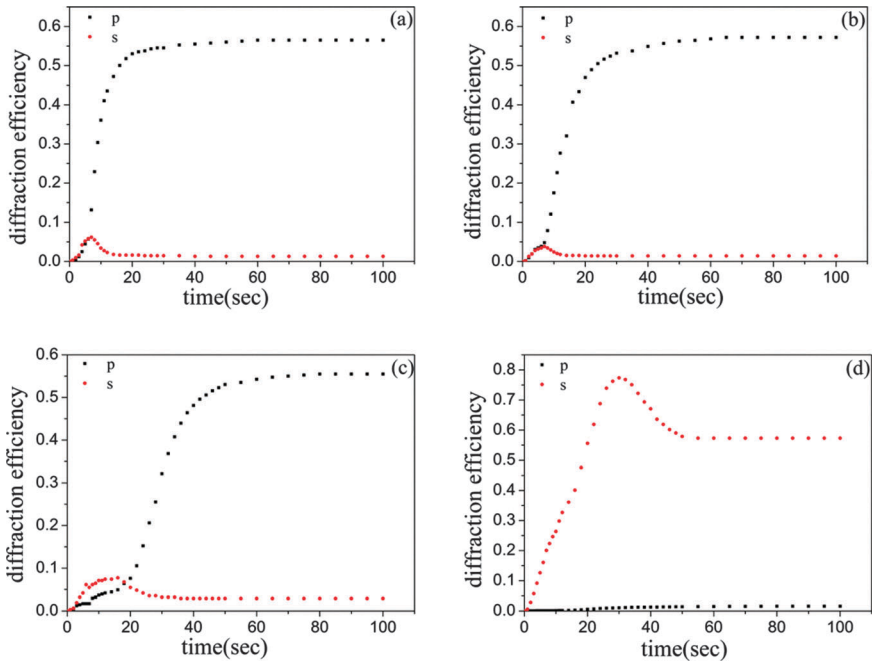

Fig. 5 Real time diffraction efficiency for p polarization (square) and s polarization (sphere) for (a) **a1** (b) **a2**, (c) **b1** and (d) **b2**, respectively.

19.1 and 1/35.8, respectively. This also means that the surface anchoring effect of the alignment PI layer is dominant in **b2**, which makes the majority of phase separated LCs to be aligned in the designed rubbing direction, as indicated in Fig. 1b.

In order to understand the difference of diffraction efficiency in **b2**, we adopt a coordinate system with x in the direction of the grating vector and y perpendicular to the cell surface. The diffraction efficiency for each polarization at the Bragg angle (θ_B) follows the equations[18]

$$\eta_p = \sin^2 \frac{\pi d\left(\varepsilon_{1x}\cos^2\theta_B - \varepsilon_{1y}\sin^2\theta_B\right)}{2n\lambda_0\cos\theta_B} \quad (1)$$

$$\eta_s = \sin^2 \frac{\pi d\varepsilon_{1z}}{2n\lambda_0\cos\theta_B} \quad (2)$$

where ε_{1i} ($i = x, y, z$) is the diagonal components of the relative permittivity modulation tensor, d is the cell gap, n is the average refractivity of the grating and λ_0 is the wavelength of the probe light (633 nm, He–Ne laser). θ_B is 20° in our experiment. As the value of θ_B is small, eqn (1) and (2) can be simplified as

$$\eta_p = \sin^2 \frac{\pi d\varepsilon_{1x}}{2n\lambda_0} \quad (3)$$

$$\eta_s = \sin^2 \frac{\pi d\varepsilon_{1z}}{2n\lambda_0} \quad (4)$$

We can see that, as the refractive index of the pure polymer (n_p = 1.525 for mixture A, n_p = 1.529 for mixture B, both measured by an Abbe refractometer) is close to the ordinary refractive index of the LC (n_o = 1.522), the change of the diffraction efficiency in s or p polarization state is mainly related to the extraordinary refractive index of the LC, *i.e.*, the orientation of the phase seperated LC molecules. From eqn (3) and (4) we can conclude that the reason that η_p or η_s increases with curing time is due to the extent to which the LC is aligned along the x axis (for η_p increasing case, Fig. 1a) or the z axis (for η_s increasing case, Fig. 1b).

On the other hand, the amplitude of the HPDLC diffraction efficiency is related to the refractive index difference between the LC and the polymer. The refractive index difference Δn can be deduced by the Kogelnik isotropic coupled wave theory[19]

$$\Delta n = \frac{\lambda_0\cos\theta_B \arcsin\sqrt{\eta_s}}{\pi d} \quad (5)$$

From eqn (5), we can note that higher η_s can be due to a larger refractive index difference, which will give more effective light feedback while pumping. It also shows that the more the LC molecules aligned along the z axis, the better the feedback for the lasing output. According to eqn (5) and measured η_s, the refractive index modulation Δn can be increased from 0.0036 (in sample **a1**) to a relatively high value of 0.0236 (in sample **b2**).

3.3 Driving voltage of the HPDLC

In HPDLCs, the surface anchoring effect of the polymer plays a key role in dictating the electro-optical properties.[20] If the anchoring strength between the polymer and the phase separated LC molecules is weak, a smaller driving voltage is required to re-orient the LC molecules with the applied field. In this work, there is a competitive relationship between surface anchoring of the polymer filaments or fibers in the rich-LC region (indicated in Fig. 1) and the anchoring effect of the alignment PI layer for samples **a2** and **b2**. Fig. 6 shows the comparison of the diffraction efficiency as a function of the driving electric field for samples **a1**–**b2**. The driving electric field E_{90} is defined here as the electric field required for attaining 90% diffraction of the first order

Published on 08 May 2015. Downloaded by Changchun Institute of Optics, Fine Mechanics and Physics, CAS on 29/05/2016 11:59:29.

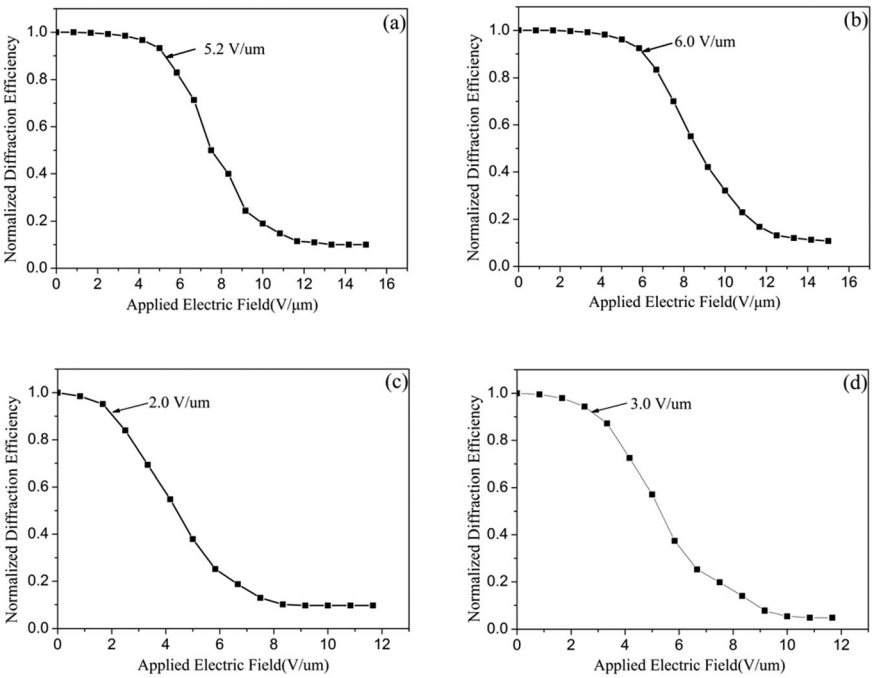

Fig. 6 Diffraction efficiency as a function of the applied electric field for (a) **a1**, (b) **a2**, (c) **b1** and (d) **b2**, respectively.

diffraction light from 100% (without applying electric field). The E_{90} values of samples **a1**, **a2** and **b1** are 5.2 V μm^{-1}, 6.0 V μm^{-1}, and 2.0 V μm^{-1}, respectively and the E_{90} of sample **b2** is 3.0 V μm^{-1}. The results indicate that the surface anchoring energies of the polymer in samples **a1** and **a2** are greater than those in samples **b1** and **b2**. We think that it is caused by different functionalities of the monomers, meaning that the multifunctional monomer will produce more polymer filaments in rich-LC regions and more anchoring energy than the lower functional monomer. Because of the monomer with lower functionality (mixture B), the surface anchoring strength of the polymer is much smaller. Therefore the alignment PI layer in sample **b2** can be dominant for the orientation of phase separated LC molecules. Such orientation of the LC will help in increasing Δn to larger values so that the lasing output threshold can be lowered when pumping because of more efficient light feedback.

3.4 Lasing output

The samples were then photo-pumped to investigate the lasing output for DFB laser application. The pumping laser wavelength was 532 nm and the pumping direction was normal to the glass substrate of the sample. The lasing output from our samples was around 630 nm. The DFB lasing wavelength λ_{las} from the device should satisfy the Bragg condition[21] $m\lambda_{las} = 2n_{eff}\Lambda$, where n_{eff} is the effective refractive index of the laser mode and m is the Bragg order, which was selected as 3 for each sample in this work. There were four lasing output beams with equal intensity from one sample and each beam was emitted at $\sim 32^{\circ}$ with respect to the normal of the glass plane for 3rd Bragg order DFB laser. The emitted lasing output beams are totally TE polarized.

Fig. 7 shows the dependence of output energy on the input energy for samples **a1–b2**. The threshold of the lasing output was obtained by the intersection of the linear fitting curve. The threshold is 0.71 μJ (*i.e.*, pump energy density 0.142 mJ cm^{-2} or perk power density per pump laser pulse 17.75 kW cm^{-2}, the same as below) for sample **a1**, 0.74 μJ (0.148 mJ cm^{-2} or 18.5 kW cm^{-2}) for sample **a2**, and 0.68 μJ (0.136 mJ cm^{-2} or 17 kW cm^{-2}) for sample **b1**. The conversion efficiency of pump input to the lasing output of samples **a1**, **a2** and **b1** are 2.3%, 2.5% and 1.9%, respectively. The values of both threshold and conversion efficiency of the three samples are similar. However, the lasing output properties of sample **b2** were greatly improved, as shown in Fig. 7d. The value of refractive index contrast is improved from 0.0036 (sample **a1**) to 0.0236. The threshold was decreased to 0.25 μJ (0.05 mJ cm^{-2} or 6.25 kW cm^{-2}) and the conversion efficiency was increased to 4.6%. The insets in Fig. 7 show the corresponding lasing spectra of samples **a1–b2**, respectively. Lasing with a narrow linewidth was observed and their full width at half maximum (FWHM) was 0.5–0.6 nm, which showed that the small difference of the lasing wavelengths in samples **a1** and **b1** can be attributed to the different kinds of mixtures being used. The lasing peak changes from 630.4 nm (sample **b1**) to 632.2 nm (sample **b2**) can be attributed to the difference in the average refractive index in the HPDLC grating due to different orientation of LC molecules caused by the PI alignment layer.

These results show that the lasing threshold can be lowered and the conversion efficiency can be increased by the rubbed PI layer to control the phase separated LCs aligned in the preferred direction in the sample with low functionality of the monomer mixture. The reason is that when the phase separated LC is aligned along the rubbing direction (z), the refractive

 This journal is © The Royal Society of Chemistry 2015

Published on 08 May 2015. Downloaded by Changchun Institute of Optics, Fine Mechanics and Physics, CAS on 29/05/2016 11:59:29.

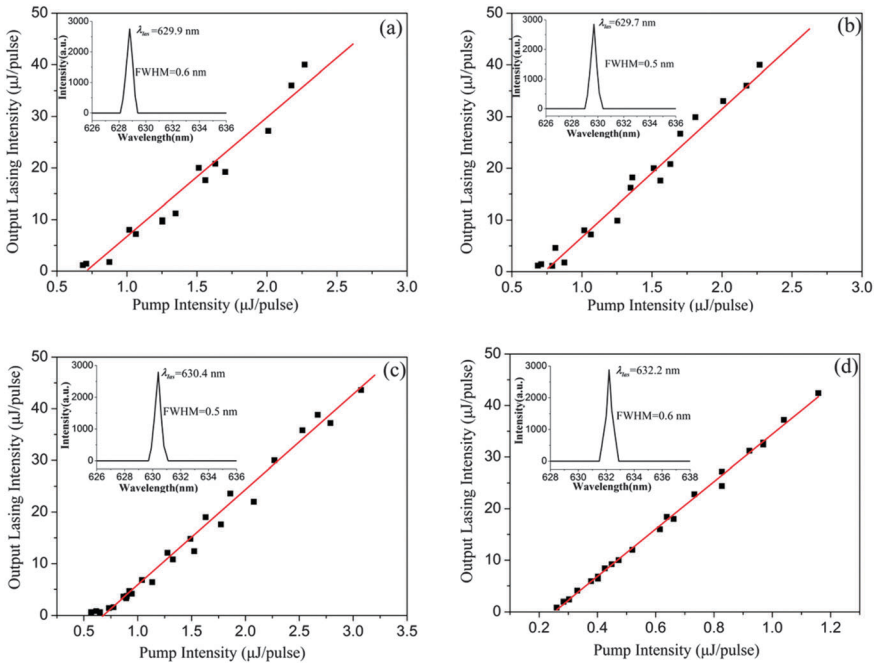

Fig. 7 Lasing output intensity as a function of pump intensity for the DFB laser: (a) **a1**, (b) **a2**, (c) **b1** and (d) **b2**. The insets show the corresponding lasing spectra, respectively.

index difference in the grating vector direction (x) comes from the polymer (for example, n_p = 1.529 for mixture B) and the LC extraordinary refractive index (n_e), which was measured to be 0.0236 in sample **b2**. Whereas in sample **a1**, the refractive index difference in the grating vector direction is 0.0036 as the phase separated LC is aligned along the grating vector direction and the refractive index of the LC is the ordinary refractive index (n_o, and $n_o < n_e$) in that case. The bigger the refractive index in the grating vector direction (the lasing feedback direction), the better the lasing feedback performance. Therefore the lasing threshold and conversion efficiency can be enhanced in this work.

4. Conclusions

In this paper, we studied the effects of the alignment PI layer on lasing output threshold and conversion efficiency based on HPDLC/core-layer/glass-substrate laser configuration. The effect of different monomers, the orientation of the LC molecules in different HPDLCs and the lasing output properties were investigated. The results indicate that the surface anchoring energy of the polymer in the HPDLC can be suppressed by using a lower functional monomer and a rubbing PI alignment layer on the substrate, making LC molecules align along the designed rubbing direction. In this way, we greatly lowered the lasing output threshold and increased conversion efficiency. The obtained HPDLC also has lower light loss, higher diffraction efficiency and lower driving voltage, which is boosted as more effectively, external light feedback layer for organic semiconducting lasers.

Acknowledgements

The authors would like to thank the National Natural Science Foundation of China (11174274, 11204299, 61377032, and 61378075) for the support.

References

1 (*a*) H. H. Telle, A. G. Urena and R. J. Donovan, *Laser Chemistry: Spectroscopy, Dynamics and Applications*, John Wiley & Sons, West Sussex, 2007; (*b*) W. M. Steen and J. Mazumder, *Lasers Material Processing (4th Edition)*, Springer, London, 2010; (*c*) N. Tessler, *Adv. Mater.*, 1999, **11**, 363–370; (*d*) J. Clark and G. Lanzani, *Nat. Photonics*, 2010, **4**, 438–446.

2 Y. Yang, G. A. Turnbull and I. D. W. Samuel, *Appl. Phys. Lett.*, 2008, **92**, 163306.

3 (*a*) T. Riedl, T. Rabe, H.-H. Johannes, W. Kowalsky, J. Wang, T. Weimann, P. Hinze, B. Nehls, T. Farrell and U. Scherf, *Appl. Phys. Lett.*, 2006, **88**, 241116; (*b*) C. Karnutsch, M. Stroisch, M. Punke, U. Lemmer, J. Wang and T. Weimann, *IEEE Photonics Technol. Lett.*, 2007, **19**, 741–743.

4 (*a*) M. D. McGehee and A. J. Heeger, *Adv. Mater.*, 2000, **12**, 1655–1668; (*b*) D. T. McQuade, A. E. Pullen and T. M. Swager, *Chem. Rev.*, 2000, **100**, 2537–2574.

5 S. Klinkhammer, X. Liu, K. Huska, Y. S. Vanderheiden, S. Valouch, C. Vannahme, S. Brase, T. Mappes and U. Lemmer, *Opt. Express*, 2012, **20**, 6357–6364.

6 R. Xia, G. Heliotis, P. Stavrinou and D. Bradley, *Appl. Phys. Lett.*, 2005, **87**, 031104.

7 M. G. Ramirez, P. G. Boj, V. Navarro-Fuster, I. Vragovic, J. M. Villalvilla, I. Alonso, V. Trabadelo, S. Merino and M. A. Diaz-Garcia, *Opt. Express*, 2011, **19**, 22443–22454.

Published on 08 May 2015. Downloaded by Changchun Institute of Optics, Fine Mechanics and Physics, CAS on 29/05/2016 11:59:29.

8 B. Wenger, N. Tetreault, M. E. Welland and R. H. Friend, *Appl. Phys. Lett.*, 2010, **97**, 193303.
9 M. Gaal, C. Gadermaier, H. Plank, E. Moderegger, A. Pogantsch, G. Leising and E. J. W. List, *Adv. Mater.*, 2003, **15**, 1165–1167.
10 T. Zhai, X. Zhang, Z. Pang and F. Dou, *Adv. Mater.*, 2011, **23**, 1860–1864.
11 I. D. W. Samuel and G. A. Turnbull, *Chem. Rev.*, 2007, **107**, 1272–1295.
12 G. Heliotis, R. Xia, G. A. Turnbull, P. Andrew, W. L. Barnes, I. D. Samuel and D. D. Bradley, *Adv. Funct. Mater.*, 2004, **14**, 91–97.
13 (*a*) Z. Diao, L. Xuan, L. Liu, M. Xia, L. Hu, Y. Liu and J. Ma, *J. Mater. Chem. C*, 2014, **2**, 6177–6182; (*b*) W. Huang, Z. Diao, Y. Liu, Z. Peng, C. Yang, J. Ma and L. Xuan, *Org. Electron.*, 2012, **13**, 2307–2311.
14 (*a*) T. J. Bunning, L. V. Natarajan, V. P. Tondiglia and R. L. Sutherland, *Annu. Rev. Mater. Sci.*, 2000, **30**, 83–115; (*b*) R. L. Sutherland, V. P. Tondiglia, L. V. Natarajan, T. J. Bunning and W. W. Adams, *Appl. Phys. Lett.*, 1994, **64**, 1074–1076; (*c*) C. Y. Li, M. J. Birnkrant, L. V. Natarajan, V. P. Tondiglia, P. F. Lloyd, R. L. Sutherland and T. J. Bunning, *Soft Matter*, 2005, **1**, 238–242; (*d*) Y. J. Liu, Y.-C. Su, Y.-J. Hsu and V. K. Hsiao, *J. Mater. Chem.*, 2012, **22**, 14191–14195; (*e*) Y. J. Liu, H. T. Dai and X. W. Sun, *J. Mater. Chem.*, 2011, **21**, 2982–2986; (*f*) L. De Sio, L. Ricciardi, S. Serak, M. La Deda, N. Tabiryan and C. Umeton, *J. Mater. Chem.*, 2012, **22**, 6669–6673; (*g*) R. Caputo, L. De Sio, A. Veltri, C. Umeton and A. V. Sukhov, *Opt. Lett.*, 2004, **29**, 1261–1263; (*h*) V. K. S. Hsiao, K.-T. Yong, A. N. Cartwright, M. T. Swihart, P. N. Prasad, P. F. Lloyd and T. J. Bunning, *J. Mater. Chem.*, 2009, **19**, 3998–4003.
15 (*a*) J. Ma, W. Huang, L. Xuan and H. Yokoyama, in *Optical Properties of Functional Polymers and Nano Engineering Applications*, ed. V. Jain and A. Kokil, CRC, 2014; (*b*) L. Liu, W. Huang, Z. Diao, Z. Peng, Q. q. Mu, Y. Liu, C. Yang, L. Hu and L. Xuan, *Liq. Cryst.*, 2014, **41**, 145–152; (*c*) Z. Diao, W. Huang, Z. Peng, Q. Mu, Y. Liu, J. Ma and L. Xuan, *Liq. Cryst.*, 2014, **41**, 239–246; (*d*) Z. Diao, S. Deng, W. Huang, L. Xuan, L. Hu, Y. Liu and J. Ma, *J. Mater. Chem.*, 2012, **22**, 23331–23334; (*e*) W. Huang, Z. Diao, L. Yao, Z. Cao, Y. Liu, J. Ma and L. Xuan, *Appl. Phys. Express*, 2013, **6**, 022702; (*f*) W. Huang, Y. Liu, Z. Diao, C. Yang, L. Yao, J. Ma and L. Xuan, *Appl. Opt.*, 2012, **51**, 4013–4020.
16 V. K. S. Hisao, C. Lu, G. S. He, M. Pan, A. N. Cartwright, P. N. Prasad, R. Jakubiak, R. A. Vaia and T. J. Bunning, *Opt. Express*, 2005, **13**, 3787–3794.
17 (*a*) R. T. Pogue, L. V. Natarajan, S. A. Siwecki, V. P. Tondiglia, R. L. Sutherland and T. J. Bunning, *Polymer*, 2000, **41**, 733–741; (*b*) M. D. Sarkar, J. Qi and G. P. Crawford, *Polymer*, 2002, **43**, 7335–7344.
18 J. J. Butler, M. S. Malcuit and M. A. Rodriguez, *J. Opt. Soc. Am. B*, 2002, **19**, 183–189.
19 H. Kogelnik, *Bell Syst. Tech. J.*, 1969, **69**, 2909–2946.
20 (*a*) R. Jakubiak, V. P. Tondiglia, L. V. Natarajan, R. L. Sutherland, P. Lloyd, T. J. Bunning and R. A. Vaia, *Adv. Mater.*, 2005, **17**, 2807–2811; (*b*) R. Jakubiak, T. J. Bunning, R. A. Vaia, L. V. Natarajan and V. P. Tondiglia, *Adv. Mater.*, 2003, **15**, 241–244; (*c*) K. K. Vardanyan, J. Qi, J. N. Eakin, M. D. Sarkar and G. P. Crawford, *Appl. Phys. Lett.*, 2002, **81**, 4736–4738; (*d*) H. Ren and S. T. Wu, *J. Appl. Phys.*, 2002, **92**, 797–800; (*e*) J. Ma, L. Shi and D.-K. Yang, *Appl. Phys. Express*, 2010, **3**, 021702; (*f*) S. E. Hicks, S. P. Hurley, Y. C. Yang and D.-K. Yang, *Soft Matter*, 2013, **9**, 3834–3839; (*g*) M. E. McConney, T. J. White, V. P. Tondiglia, L. V. Natarajan, D.-K. Yang and T. J. Bunning, *Soft Matter*, 2012, **8**, 318–323; (*h*) D.-K. Yang and S.-T. Wu, *Fundamentals of Liquid Crystal Devices*, John Wiley & Sons Inc., New York, 2006.
21 H. Kogelnik and C. V. Shank, *J. Appl. Phys.*, 1972, **43**, 2327–2335.

 This journal is © The Royal Society of Chemistry 2015